

A Refined Sinus Finite Element Model for the Analysis of Piezoelectric-Laminated Beams

S. B. BEHESHTI-AVAL,¹ M. LEZGY-NAZARGAH,¹ P. VIDAL^{2,*} AND O. POLIT²

¹*Department of Civil Engineering, Khajeh Nasir Toosi University of Technology, Tehran, Iran*

²*LEME-EA 4416, Universite Paris Ouest, 50 rue de Sévres, 92410 Ville d'Avray, France*

ABSTRACT: A three-noded beam finite element is developed for the analysis of composite-laminated beams with distributed piezoelectric sensor/actuator layers. The mechanical part of the proposed element is based on the refined sinus model. This element does not require shear correction factor and ensures continuity conditions for displacements, transverse shear stresses as well as boundary conditions on the upper and lower surfaces of the beam. This conforming finite element is totally free of shear locking, and the number of mechanical unknowns is independent of the number of layers. For each piezoelectric layer, a high-order electrical potential field is considered. The virtual work principle leads to a derivation that could include dynamic analysis. However, in this study, only static problems have been considered. Comparison of numerical results obtained from this formulation with previous works shows that the present finite element is suitable for predicting fully coupled behaviors of both thick and thin smart-laminated beams under mechanical and electrical loadings.

Key Words: finite element, composite beams, piezoelectric layers, refined sinus model.

INTRODUCTION

FUTURE engineering research is inclined toward structures that are able to sense, respond, and minimize the effects of applied disturbance on them. This class of structures is generally called smart structures. Piezoelectric materials have been widely used in the form of sensors and actuators in order to self-respond to structures. Thanks to small dimensions, it is possible to use many piezoelectric patches as sensors and actuators, without causing significant changes in dynamic properties of the main structure. In the application of sensors, mechanically induced deformations can be determined by measuring the induced electrical potential, whereas in the application of actuators, deformations can be controlled by introducing an appropriate electric potential. An overview on applications of smart structures can be found in the study carried by Chopra (2002) and Gaudenzi (2009).

Various mathematical models developed for structures containing piezoelectric sensors and actuators can be classified into two broad categories including induced strain models and coupled electromechanical models. An overview on the modeling of piezoelectric

structures is given in Benjeddou (2000), Saravanan and Heyliger (1999), and Carrera and Boscolo (2007). Also, see Gaudenzi (2009).

The induced strain models use approximate theories in order to incorporate external forces associated with the piezoelectric actuators. The electric potential is neglected as a state variable in the formulation; therefore, these models cannot capture the coupled mechanical and electrical responses and are only limited to predict the actuator behavior of piezoelectric materials (Crawley and de Luis, 1987; Tzou and Gadre, 1989; Wang and Rogers, 1991; Sung et al., 1996).

Compared to the induced strain models, the coupled electromechanical models provide a more consistent representation of both the sensor and actuator responses of piezoelectric materials, incorporating both the displacements and the electric potentials as the state variables in the formulation. Piezoelectric three-dimensional (3D) finite elements (FEs) have been proposed early by Allik and Hughes (1970), Tzou and Tseng (1990), and Xu et al. (1995). However, the cost of the 3D analysis is relatively high, and it will become a problem when piezoelectric layers are thin compared to the structure size.

In order to overcome these restrictions, several theories for laminated structures including piezoelectric elements exist in the literature. The electric part is usually modeled by a layerwise (LW) approach (Reddy, 1993); therefore, the discussion concerns only the mechanical approach.

*Author to whom correspondence should be addressed.
E-mail: Philippe.Vidal@u-paris10.fr
Figures 1 and 4–14 appear in color online: <http://jim.sagepub.com>

The following classification is associated with the dependence on the number of mechanical degrees of freedom (DOFs) with respect to the number of layers:

- The equivalent single layer (ESL) approach: the number of unknowns is independent of the number of layers, but continuity of transverse shear and normal stresses is often violated at layer interfaces. This approach is called ‘hybrid’ or ‘mixed’ in the literature. We can distinguish classical laminate theory (CLT), first-order shear deformation theory (FSDT) (Suleman and Venkayya (1995), Sheikh et al. (2001), and Wang (2004) for plates), and higher order theories: the third-order shear deformation theory has been carried out by Chee et al. (1999) (beams), and Shu (2005), Thornburgh and Chattopadhyay (2002), Fukunaga et al. (2001), and Mitchell and Reddy (1995) (plates) for instance.
- The LW approach: the number of DOFs depends on the number of layers. This theory aims at overcoming the ESL shortcoming by allowing discontinuity of out-of-plane stresses on the interface layers. See for instance, Saravanos and Heyliger (1995), Kusculuoglu et al. (2004), and Plagianakos and Saravanos (2005) for beams, Semedo Garcao et al. (2004), Garcia Lage et al. (2004a, b), Heyliger and Saravanos (1994), Saravanos et al. (1997), and Robaldo et al. (2006), etc., for plates, and Tzou and Ye (1996) for shells.

Note that an extensive assessment has been provided by Saravanos and Heyliger (1999).

In this framework, refined models have been developed in order to improve the accuracy of ESL models while avoiding the computational burden of the LW approach. Starting from a refined LW description, taking into account physical considerations and after some algebraic transformations, the number of unknowns becomes independent of the number of layers. This type of approach has been carried out by Ambartsumyan (1969). The resulting model can be classified as a zig-zag one (see the historical review of Carrera (2003)). In the framework of electromechanical problems, Oh and Cho (2004) have extended the third-order zig-zag model. Also, note the recent works for beams (Kapuria, 2001; Kapuria and Alam, 2006) and plates (Kapuria, 2004).

Finally, the so-called advanced models based on principle of virtual displacement (PVD) or Reissner’s mixed variational theorem (RMVT), and Carrera unified formulation (CUF) must be referred here. Different types of interlaminar continuity can be considered: transverse shear/normal stresses and/or transverse electric displacement. For the most recent works on multilayered piezoelectric structures, readers can refer to D’Ottavio and Kröplin (2006) and Carrera and Nali (2009) for plates, and Carrera and Brischetto (2007) for shells.

In this article, a refined sinus beam FE is presented for the prediction of fully coupled behavior of smart rectangular laminated beams under electromechanical conditions. This element is based on the sinus model introduced by Touratier (1991). Then, it was extended to take into account the interlaminar continuity of the transverse shear stresses by Polit and Touratier (2000) for plates, and by Dau et al. (2004) for shells. The coupling with the piezoelectric effect is carried out by Ossadzow-David and Touratier (2004) and Fernandes and Pouget (2003) using an analytical approach. The original sinus model has been enriched by Vidal and Polit (2008) by introducing a layer refinement in the kinematics, and then extended to thermal effects (Vidal and Polit, 2009). In this framework, this study is focused on the extension of these last works of the piezoelectric effect.

This beam element is a three-nodded element which satisfies the continuity conditions between layers of laminate for displacements, transverse shear stress, and the free conditions at the top and bottom surfaces of the beam. The element is totally free of shear locking (cf. Vidal and Polit, 2008) and has finally four independent generalized displacements: three displacements and one rotation. Concerning the electrical part, a high-order electrical potential field is considered. The advantage of this electrical potential field is that it satisfies the boundary conditions of applied voltage. This high-order electrical potential also allows dealing with the conjuncture conditions between two piezoelectric layers using the electric field at the interface. The results obtained with this FE are in good agreement with available published reference solutions. This efficient FE is simple and has a low cost compared to layer-wise theory or 3D models from commercial softwares.

MATHEMATICAL FORMULATION

Geometry and Coordinate System

The considered beam has a rectangular uniform cross-section of height h , width b , and is assumed to be straight. The beam is made of NC layers of different linearly elastic materials. Each layer may be piezoelectric (actuators/sensors) or non-piezoelectric. The laminated beam and Cartesian coordinate system (x_1, x_2, z) are shown in Figure 1. As shown in this figure, the x_1 , x_2 , and z axes are respectively along the central line, width, and thickness of the beam. This study is based upon a displacement approach for geometrically linear elastic beams.

Constitutive and Governing Coupled Equations

In this study, the non-piezoelectric materials are assumed to be orthotropic and the general type of

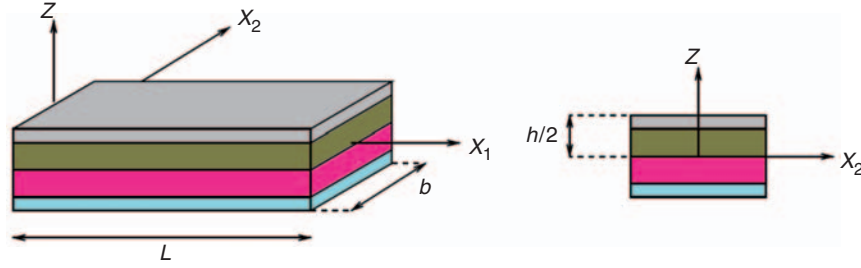


Figure 1. The laminated piezoelectric beam and coordinate system.

piezoelectric materials is “orthorhombic-class $mm2$.” Considering this assumption, the constitutive equations of a piezoelectric material in its material axis system can be expressed as:

$$\begin{Bmatrix} \sigma_{xx} \\ \sigma_{yy} \\ \sigma_{zz} \\ \tau_{yz} \\ \tau_{xz} \\ \tau_{xy} \end{Bmatrix} = \begin{bmatrix} c_{11} & c_{12} & c_{13} & 0 & 0 & c_{16} \\ c_{21} & c_{22} & c_{23} & 0 & 0 & c_{26} \\ c_{31} & c_{32} & c_{33} & 0 & 0 & c_{36} \\ 0 & 0 & 0 & c_{44} & c_{45} & 0 \\ 0 & 0 & 0 & c_{54} & c_{55} & 0 \\ c_{61} & c_{62} & c_{63} & 0 & 0 & c_{66} \end{bmatrix} \begin{Bmatrix} \varepsilon_{xx} \\ \varepsilon_{yy} \\ \varepsilon_{zz} \\ \gamma_{yz} \\ \gamma_{xz} \\ \gamma_{xy} \end{Bmatrix} - \begin{bmatrix} e_{11} & e_{21} & e_{31} \\ e_{12} & e_{22} & e_{32} \\ e_{13} & e_{23} & e_{33} \\ e_{14} & e_{24} & e_{34} \\ e_{15} & e_{25} & e_{35} \\ e_{16} & e_{26} & e_{36} \end{bmatrix} \begin{Bmatrix} E_x \\ E_y \\ E_z \end{Bmatrix} \quad (1)$$

$$\begin{Bmatrix} D_x \\ D_y \\ D_z \end{Bmatrix} = \begin{bmatrix} e_{11} & e_{12} & e_{13} & e_{14} & e_{15} & e_{16} \\ e_{21} & e_{22} & e_{23} & e_{24} & e_{25} & e_{26} \\ e_{31} & e_{32} & e_{33} & e_{34} & e_{35} & e_{36} \end{bmatrix} \begin{Bmatrix} \varepsilon_{xx} \\ \varepsilon_{yy} \\ \varepsilon_{zz} \\ \gamma_{yz} \\ \gamma_{xz} \\ \gamma_{xy} \end{Bmatrix} + \begin{bmatrix} \chi_{11} & \chi_{12} & \chi_{13} \\ \chi_{21} & \chi_{22} & \chi_{23} \\ \chi_{31} & \chi_{32} & \chi_{33} \end{bmatrix} \begin{Bmatrix} E_x \\ E_y \\ E_z \end{Bmatrix} \quad (2)$$

where D_i is the electric displacement vector components, E_i the electric field vector, and c_{ij} , e_{ij} , χ_{ij} the elastic, piezoelectric, and dielectric material constants.

In a laminated beam with small width, the following assumptions are made:

$$\sigma_{zz} \cong 0, \quad \sigma_{yy} \cong 0, \quad \tau_{yz} \cong 0, \quad \tau_{xy} \cong 0, \quad E_y \cong 0 \quad (3)$$

Using the conditions (3), the constitutive relations (1) and (2) reduce to:

$$\begin{aligned} \bar{\sigma} &= \bar{C}\bar{\varepsilon} - \bar{e}\bar{E} \\ \bar{D} &= \bar{e}^T\bar{\varepsilon} + \bar{\chi}\bar{E} \end{aligned} \quad (4)$$

where

$$\begin{aligned} \bar{\sigma} &= \begin{bmatrix} \sigma_{xx} \\ \tau_{xz} \end{bmatrix}, \quad \bar{D} = \begin{bmatrix} D_x \\ D_z \end{bmatrix} \\ \bar{C} &= \begin{bmatrix} c_{11} & 0 \\ 0 & c_{55} \end{bmatrix} - \begin{bmatrix} c_{12} & c_{13} & c_{16} & 0 \\ 0 & 0 & 0 & c_{54} \end{bmatrix} \\ &\quad \times \begin{bmatrix} c_{22} & c_{23} & c_{26} & 0 \\ c_{32} & c_{33} & c_{36} & 0 \\ c_{62} & c_{63} & c_{66} & 0 \\ 0 & 0 & 0 & c_{44} \end{bmatrix}^{-1} \begin{bmatrix} c_{21} & 0 \\ c_{31} & 0 \\ c_{61} & 0 \\ 0 & c_{45} \end{bmatrix} \\ \bar{e} &= \begin{bmatrix} e_{11} & e_{31} \\ e_{15} & e_{35} \end{bmatrix} - \begin{bmatrix} c_{12} & c_{13} & c_{16} & 0 \\ 0 & 0 & 0 & c_{54} \end{bmatrix} \\ &\quad \times \begin{bmatrix} c_{22} & c_{23} & c_{26} & 0 \\ c_{32} & c_{33} & c_{36} & 0 \\ c_{62} & c_{63} & c_{66} & 0 \\ 0 & 0 & 0 & c_{44} \end{bmatrix}^{-1} \begin{bmatrix} e_{12} & e_{32} \\ e_{13} & e_{33} \\ e_{16} & e_{36} \\ e_{14} & e_{34} \end{bmatrix} \\ \bar{\chi} &= \begin{bmatrix} \chi_{11} & \chi_{13} \\ \chi_{31} & \chi_{33} \end{bmatrix} + \begin{bmatrix} e_{12} & e_{13} & e_{16} & e_{14} \\ e_{32} & e_{33} & e_{36} & e_{34} \end{bmatrix} \\ &\quad \times \begin{bmatrix} c_{22} & c_{23} & c_{26} & 0 \\ c_{32} & c_{33} & c_{36} & 0 \\ c_{62} & c_{63} & c_{66} & 0 \\ 0 & 0 & 0 & c_{44} \end{bmatrix}^{-1} \begin{bmatrix} e_{12} & e_{32} \\ e_{13} & e_{33} \\ e_{16} & e_{36} \\ e_{14} & e_{34} \end{bmatrix} \end{aligned}$$

The principle of virtual work for the piezoelectric medium of volume Ω and regular boundary surface Γ can be written as:

$$\begin{aligned} & - \int_{\Omega} \sigma_{ij} \delta \varepsilon_{ij} d\Omega + \int_{\Gamma} F_i \delta u_i dS + \int_{\Omega} f_i \delta u_i d\Omega + f_{ci} \delta u_i \\ & - \int_{\Omega} \rho \ddot{u}_i \delta u_i d\Omega + \int_{\Omega} D_i \delta E_i d\Omega - \int_{\Gamma} \bar{Q} \delta \phi dS - \int_{\Omega} \bar{q} \delta \phi d\Omega = 0 \end{aligned} \quad (5)$$

where F_i , f_i , \bar{q} , and \bar{Q} are surface force components, mechanical body force components, electrical body charge, and surface charge, respectively. δu_i and $\delta \phi$ are admissible virtual displacement and potential. ρ is the mass density and f_{ci} the components of concentrated loads.

Substituting Equation (4) in Equation (5) allows us to deduce the formulation, where u_i and ϕ are the unknowns. The obtained equation is a good starting point for a FE formulation.

Displacement and Strain Fields

The displacement field used in this model is given by Vidal and Polit (2008):

$$\begin{aligned} u_1(x_1, x_2, z, t) &= u(x_1, t) - zw(x_1, t)' + f(z)(\omega_3(x_1, t) + w(x_1, t)') \\ &+ \sum_{k=1}^{NC} (\bar{u}_{loc}^k(x_1, z, t) + \hat{u}_{loc}^k(x_1, z, t))(H(z - z_k) \\ &- H(z - z_{k+1})) \\ u_3(x_1, x_2, z, t) &= w(x_1, t) \end{aligned} \quad (6)$$

The functions $u_1(x_1, x_2, z, t)$ and $u_3(x_1, x_2, z, t)$ represent the horizontal and vertical displacements, respectively. The subfunctions $u(x_1, t)$ and $w(x_1, t)$ are the mid-plane horizontal and vertical displacements, respectively. $\omega_3(x_1, t)$ is the shear bending rotation around the x_2 axis, and t the time.

The local functions \bar{u}_{loc}^k and \hat{u}_{loc}^k based on Legendre polynomial can be written as:

$$\bar{u}_{loc}^k(x_1, z, t) = \xi_k u_{31}^k(x_1, t) + \left(-\frac{1}{2} + \frac{3\xi_k^2}{2}\right) u_{32}^k(x_1, t) \quad (7)$$

$$\hat{u}_{loc}^k(x_1, z, t) = \left(-\frac{3\xi_k}{2} + \frac{5\xi_k^3}{2}\right) u_{33}^k(x_1, t) \quad (8)$$

where $\xi_k = a_k z - b_k$, $a_k = \frac{2}{z_{k+1} - z_k}$, and $b_k = \frac{z_{k+1} + z_k}{z_{k+1} - z_k}$. H is the heaviside function, $f(z)$ is defined by:

$$f(z) = \frac{h}{\pi} \sin\left(\frac{\pi z}{h}\right)$$

The coordinate system related to the above formulation is shown in Figure 2.

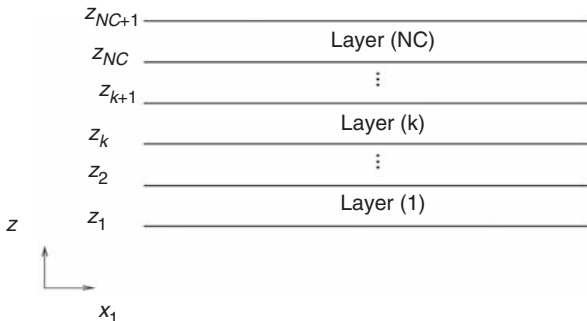


Figure 2. Coordinate system of the laminated piezoelectric beam.

CONTINUITY CONDITIONS

The following continuity conditions on displacements and interlaminar stresses must be imposed to the displacement field equations.

Displacement Continuity Conditions

The continuity conditions of displacement on the laminate interfaces should be satisfied. By applying the continuity condition on the displacement based on the so-called 1,2–3 double-superposition theory (Li and Liu, 1997), the following two equations can be deduced:

$$\bar{u}_{loc}^{(k)} = \bar{u}_{loc}^{(k-1)} \quad k = 2, \dots, NC \quad (9)$$

$$\hat{u}_{loc}^{(k)} = \hat{u}_{loc}^{(k-1)} \quad k = 2, \dots, NC \quad (10)$$

Using the above equations yields the following equations:

$$u_{32}^k = u_{31}^{k-1} + u_{32}^{k-1} + u_{31}^k \quad (11)$$

$$u_{33}^k = (-1)^{k-1} u_{33}^1 \quad (12)$$

Transverse Shear Stress Continuity

The transverse shear stress of the k th layer can be obtained as follows:

$$\begin{aligned} \tau_{13}^k &= G_k f'(z)(\omega_3 + w') + G_k a_k u_{31}^k + 3G_k \xi_k a_k u_{32}^k \\ &+ G_k \left(-\frac{3}{2} a_k + \frac{15}{2} a_k \xi_k^2\right) u_{33}^k \end{aligned} \quad (13)$$

where G_k is the shear modulus of k th layer. By imposing the transverse continuity conditions between two adjacent layers, the following recursive equations need to be satisfied:

$$\begin{aligned} G_k f'(z_k)(\omega_3 + w') + G_k a_k u_{31}^k - 3G_k a_k u_{32}^k + 6G_k a_k u_{33}^k = \\ G_{k-1} f'(z_k)(\omega_3 + w') + G_{k-1} a_{k-1} u_{31}^{k-1} + 3G_{k-1} a_{k-1} u_{32}^{k-1} \\ + 6G_{k-1} a_{k-1} u_{33}^{k-1} \quad k = 2, \dots, NC \end{aligned} \quad (14)$$

Boundary Conditions

Free shear traction conditions should be satisfied for both lower and upper surfaces. Thus, the following two boundary conditions are obtained:

$$\begin{aligned} \tau_{13}^1 \left(z = -\frac{h}{2}\right) &= G_1 f' \left(-\frac{h}{2}\right) (\omega_3 + w') + G_1 a_1 u_{31}^1 \\ &- 3G_1 a_1 u_{32}^1 + 6G_1 a_1 u_{33}^1 = 0 \end{aligned} \quad (15)$$

$$\begin{aligned} \tau_{13}^{NC} \left(z = \frac{h}{2} \right) &= G_1 f' \left(\frac{h}{2} \right) (\omega_3 + w') + G_{NC} a_{NC} u_{31}^{NC} \\ &+ 3G_{NC} a_{NC} u_{32}^{NC} + 6G_{NC} a_{NC} u_{33}^{NC} = 0 \end{aligned} \quad (16)$$

Using Equations (11) and (14), the following recursive equations are obtained:

$$u_{31}^k = A_k (\omega_3 + w') + B_k u_{31}^{k-1} + C_k u_{32}^{k-1} + D_k u_{33}^k \quad (17)$$

$$u_{32}^k = E_k (\omega_3 + w') + F_k u_{31}^{k-1} + H_k u_{32}^{k-1} + I_k u_{33}^k \quad (18)$$

The calculation of coefficients A_k , B_k , C_k , D_k , E_k , F_k , H_k , and I_k are detailed in Appendix. Substituting Equation (12) in Equation (15) yields:

$$u_{33}^k = \frac{(-1)^k f' \left(-\frac{h}{2} \right)}{6a_1} (\omega_3 + w') + \frac{(-1)^k}{6} u_{31}^1 + \frac{(-1)^{k-1}}{2} u_{32}^1 \quad (19)$$

The above equation expresses u_{33}^k with respect to u_{31}^1 , u_{32}^1 , and $(\omega_3 + w')$. Substituting Equation (19) in recursive Equations (17) and (18) allows us to deduce u_{31}^k and u_{32}^k with respect to u_{31}^1 , u_{32}^1 , and $(\omega_3 + w')$. After calculating u_{31}^{NC} , u_{32}^{NC} , and u_{33}^{NC} , respectively, from recursive Equations (17), (18), and (19) and substituting them in Equation (16), u_{32}^1 can be eliminated. Thus, Equations (17), (18), and (19) can be rewritten as:

$$\begin{cases} u_{31}^k(x_1, t) = \beta_1^k (\omega_3(x_1, t) + w(x_1, t')) + \delta_1^k u_{31}^1(x_1, t) \\ \quad k = 1, \dots, NC \\ u_{32}^k(x_1, t) = \beta_2^k (\omega_3(x_1, t) + w(x_1, t')) + \delta_2^k u_{31}^1(x_1, t) \\ \quad k = 1, \dots, NC \\ u_{33}^k(x_1, t) = \beta_3^k (\omega_3(x_1, t) + w(x_1, t')) + \delta_3^k u_{31}^1(x_1, t) \\ \quad k = 1, \dots, NC \end{cases} \quad (20)$$

where coefficients β_1^k , β_2^k , and β_3^k and δ_1^k , δ_2^k , and δ_3^k are obtained from the procedure described above. These coefficients are only dependent on the shear modulus and z -axis coordinate of layers. Finally, the four unknowns are u , w , ω_3 , and u_{31}^1 .

Displacement and Strain Fields

Using the usual definitions for strain, the strain equations can be derived from the displacement field:

$$\begin{aligned} \varepsilon_{11} &= u_{,1} - zw_{,11} + (\omega_{3,1} + w_{,11})F(z) + S(z)u_{31,1}^1 \\ \gamma_{13} &= (\omega_3 + w_{,1})F(z)_{,3} + S(z)_{,3}u_{31}^1 \end{aligned} \quad (21)$$

where

$$\begin{aligned} F(z) &= f(z) + \sum_{k=1}^{NC} \left(\xi_k \beta_1^k + \left(-\frac{1}{2} + \frac{3\xi_k^2}{2} \right) \beta_2^k \right. \\ &\quad \left. + \left(-\frac{3\xi_k}{2} + \frac{5\xi_k^3}{2} \right) \beta_3^k \right) \times (H(z - z_k) - H(z - z_{k+1})) \\ S(z) &= \sum_{k=1}^{NC} \left(\xi_k \delta_1^k + \left(-\frac{1}{2} + \frac{3\xi_k^2}{2} \right) \delta_2^k + \left(-\frac{3\xi_k}{2} + \frac{5\xi_k^3}{2} \right) \delta_3^k \right) \\ &\quad \times (H(z - z_k) - H(z - z_{k+1})) \end{aligned}$$

In order to prepare the FE approximations, the displacement and the strain Equations (6) and (21) are expressed in the following form:

$$\mathbf{u} = \mathbf{A}_u \mathbf{u}_u, \quad \boldsymbol{\varepsilon} = \mathbf{L}_u \mathbf{u}_u \quad (22)$$

where $\mathbf{u} = [u_1 \quad u_3]^T$, $\mathbf{u}_u = [u \quad w \quad \omega_3 \quad u_{31}^1]^T$, $\boldsymbol{\varepsilon} = [\varepsilon_{11} \quad \gamma_{13}]^T$, and

$$\begin{aligned} \mathbf{A}_u &= \begin{bmatrix} 1 & -z \frac{d}{dx_1} + F(z) \frac{d}{dx_1} & F(z) & S(z) \\ 0 & 1 & 0 & 0 \end{bmatrix}, \\ \mathbf{L}_u &= \begin{bmatrix} \frac{d}{dx_1} & -z \frac{d^2}{dx_1^2} + F(z) \frac{d^2}{dx_1^2} & F(z) \frac{d}{dx_1} & S(z) \frac{d}{dx_1} \\ 0 & F(z)_{,3} \frac{d}{dx_1} & F(z)_{,3} & S(z)_{,3} \end{bmatrix} \end{aligned}$$

High-Order Electric Potential

In this study, the following electric potential has been used for the k th piezoelectric layer (Jiang and Li, 2007):

$$\begin{aligned} \phi_k(x_1, x_2, \xi_k) &= L_{k1}(\xi_k) \bar{E}_{k+1}(x_1, x_2) + L_{k2}(\xi_k) \bar{E}_k(x_1, x_2) \\ &\quad + L_{k3}(\xi_k) \bar{\phi}_k(x_1, x_2) \end{aligned} \quad (23)$$

where $\bar{E}_{k+1}(x_1, x_2)$ and $\bar{E}_k(x_1, x_2)$ denote the electric field at the top and bottom surfaces, respectively. $\bar{\phi}_k(x_1, x_2)$ is the difference of electric potential between the top and bottom surfaces. $L_{ki}(\xi_k)$ ($i = 1, 2, 3$) are the interpolation functions as follows:

$$\begin{cases} L_{k1} = -\frac{1}{8}(\xi_k + 1)^2(\xi_k - 1)(z_{k+1} - z_k) \\ L_{k2} = -\frac{1}{8}(\xi_k + 1)(\xi_k - 1)^2(z_{k+1} - z_k) \\ L_{k3} = \frac{3}{4}(\xi_k + \frac{1}{2})^2 - \frac{1}{4}(\xi_k + \frac{1}{2})^3 - \frac{1}{2} \end{cases} \quad (24)$$

This high-order electric potential ensures the boundary condition of applied voltages. Moreover, this electric potential enables us to deal with the conjuncture conditions between two piezoelectric layers by means of the electric field at the interface. According to the definition of electric field, this one can be

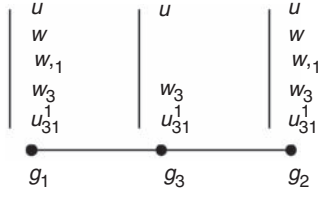


Figure 3. Mechanical representation of the laminated beam FE.

expressed as:

$$\begin{aligned} \mathbf{E}_k &= \begin{bmatrix} E_{x_1} \\ E_z \end{bmatrix}_{\text{layer } k} = - \left\{ \begin{array}{c} \frac{\partial \phi}{\partial x_1} \\ \frac{\partial \phi}{\partial z} \end{array} \right\}_k \\ &= - \begin{bmatrix} L_{k1}(\xi_k) \frac{d}{dx_1} & L_{k2}(\xi_k) \frac{d}{dx_1} & L_{k3}(\xi_k) \frac{d}{dx_1} \\ \frac{dL_{k1}}{dz} & \frac{dL_{k2}}{dz} & \frac{dL_{k3}}{dz} \end{bmatrix} \begin{Bmatrix} \bar{E}_{k+1} \\ \bar{E}_k \\ \bar{\phi}_k \end{Bmatrix} \\ &= -\mathbf{L}_\phi^k \mathbf{u}_\phi^k \end{aligned} \quad (25)$$

FE FORMULATION

FE approximations have to be defined for the variables of Equation (6). From the displacement field (Equation (6)), the transverse displacement w must be C^1 -continuous. Therefore, Hermite cubic functions are employed to interpolate transverse displacement w . Although the rotation ω_3 must be only C^0 -continuous, it is interpolated by Lagrange quadratic functions. This choice allows the same order of interpolation for both $w_{,1}$ and ω_3 in the corresponding transverse shear strain components due to bending, and enables to avoid transverse shear locking phenomenon using the field compatibility approach. Finally, u and u_{31}^1 are interpolated by Lagrange quadratic functions (Polit et al., 1994; Polit and Bruant, 2006; Vidal and Polit, 2006; Vidal and Polit, 2008). Mechanical representation of the laminated beam FE is shown in Figure 3. For the geometric approximation, Lagrange's linear interpolation is employed. The mechanical variables \mathbf{u}_u can be expressed with respect to the DOFs vector \mathbf{u}_u^e as follows:

$$\mathbf{u}_u = \mathbf{N}_u \mathbf{u}_u^e \quad (26)$$

where

$$\begin{aligned} \mathbf{u}_u^e &= \left\{ u_1 \ w_1 \ (\omega_3)_1 \ (w_{,1})_1 \ (u_{31}^1)_1 \ u_3 \ (\omega_3)_3 \right. \\ &\quad \left. (u_{31}^1)_3 \ u_2 \ w_2 \ (\omega_3)_2 \ (w_{,1})_2 \ (u_{31}^1)_2 \right\}^T \\ \mathbf{N}_u &= \begin{bmatrix} \bar{N}_1 & 0 & 0 & 0 & 0 & \bar{N}_3 & 0 & 0 & \bar{N}_2 & 0 & 0 & 0 & 0 \\ 0 & N_1 & 0 & Nd_1 & 0 & 0 & 0 & 0 & 0 & N_2 & 0 & Nd_2 & 0 \\ 0 & 0 & \bar{N}_1 & 0 & 0 & 0 & \bar{N}_3 & 0 & 0 & 0 & \bar{N}_2 & 0 & 0 \\ 0 & 0 & 0 & 0 & \bar{N}_1 & 0 & 0 & \bar{N}_3 & 0 & 0 & 0 & 0 & \bar{N}_2 \end{bmatrix} \end{aligned}$$

where $\bar{N}_i (i = 1, 2, 3)$ are the Lagrangian quadratic functions defined as

$$\begin{aligned} \bar{N}_1 &= \bar{N}_1(\xi) = -\xi(1-\xi)/2, & \bar{N}_2 &= \bar{N}_2(\xi) = \xi(1+\xi)/2 \\ \bar{N}_3 &= \bar{N}_3(\xi) = (1+\xi)(1-\xi)/2 \end{aligned} \quad (27)$$

and the Hermitian shape functions are:

$$\begin{aligned} N_1 &= N_1(\xi) = \frac{1}{4}(1-\xi)^2(2+\xi), \\ N_2 &= N_2(\xi) = \frac{1}{4}(2-\xi)(1+\xi)^2 \\ Nd_1 &= Nd_1(\xi) = \frac{l_e}{8}(1-\xi)^2(1+\xi), \\ Nd_2 &= Nd_2(\xi) = -\frac{l_e}{8}(1-\xi)(1+\xi)^2 \end{aligned} \quad (28)$$

where ξ is the local coordinate.

Using Equations (22) and (26), the displacements vector and the strain vector can be expressed as follows:

$$\begin{aligned} \mathbf{u} &= \mathbf{A}_u \mathbf{u}_u = \mathbf{A}_u \mathbf{N}_u \mathbf{u}_u^e = \mathbf{N} \mathbf{u}_u^e, \\ \boldsymbol{\varepsilon} &= \mathbf{L}_u \mathbf{u}_u = \mathbf{L}_u \mathbf{N}_u \mathbf{u}_u^e = \mathbf{B}_u \mathbf{u}_u^e \end{aligned} \quad (29)$$

where the \mathbf{N} and \mathbf{B}_u are displacement and strain interpolation matrices, respectively. Again, using the linear Lagrangian interpolation functions for $\bar{E}_k(x, y)$, $\bar{E}_{k+1}(x, y)$, and $\bar{\phi}_k(x, y)$, the vector \mathbf{u}_ϕ can be expressed as:

$$\mathbf{u}_\phi = \mathbf{N}_\phi \mathbf{u}_\phi^e \quad (30)$$

where

$$\mathbf{N}_\phi = \begin{bmatrix} N_1^0 & 0 & 0 & N_2^0 & 0 & 0 \\ 0 & N_1^0 & 0 & 0 & N_2^0 & 0 \\ 0 & 0 & N_1^0 & 0 & 0 & N_2^0 \end{bmatrix},$$

$\mathbf{u}_\phi^e = [(\bar{E}_k)_1 \ (\bar{E}_{k+1})_1 \ (\bar{\phi}_k)_1 \ (\bar{E}_k)_2 \ (\bar{E}_{k+1})_2 \ (\bar{\phi}_k)_2]^T$ and N_1^0, N_2^0 are the Lagrangian linear shape functions defined as:

$$N_1^0 = N_1^0(\xi) = (1-\xi)/2, \quad N_2^0 = N_2^0(\xi) = (1+\xi)/2 \quad (31)$$

From Equations (25) and (31), the electric field E can be expressed as:

$$\mathbf{E} = -\mathbf{L}_\phi \mathbf{u}_\phi = -\mathbf{L}_\phi \mathbf{N}_\phi \mathbf{u}_\phi^e = -\mathbf{B}_\phi \mathbf{u}_\phi^e \quad (32)$$

Substituting Equations (4), (30), (31), and (33) in Equation (5), and assembling the elementary matrices, yield the following general dynamic equation of motion:

$$\begin{bmatrix} \mathbf{M} & \mathbf{0} \\ \mathbf{0} & \mathbf{0} \end{bmatrix} \begin{bmatrix} \ddot{\mathbf{q}}(t) \\ \dot{\boldsymbol{\phi}}(t) \end{bmatrix} + \begin{bmatrix} \mathbf{K}_{qq} & \mathbf{K}_{q\phi} \\ \mathbf{K}_{\phi q} & \mathbf{K}_{\phi\phi} \end{bmatrix} \begin{bmatrix} \mathbf{q}(t) \\ \boldsymbol{\phi}(t) \end{bmatrix} = \begin{bmatrix} \mathbf{F}_q(t) \\ \mathbf{F}_\phi(t) \end{bmatrix} \quad (33)$$

Table 1. Main features of different FE models.

Number of DOFs per node or (element)		Element/number of nodes	Interlayer continuity conditions	Number of generalized unknowns		Models
Electrical	Mechanical			electrical	mechanical	
NCP + 1	2 × NC + 2	Beam/2	Not considered	NCP + 1	2 × NC + 2	Saravanos and Heyliger (1995)
NCP + 1	4	Beam/2	Not considered	NCP + 1	3	Chee et al. (1999)
(NCP)	5	Plate/9	Not considered	NCP	5	Fukunaga et al. (2001), nine-node element
(NCP)	7	Plate/4	Not considered	NCP	5 + 2	Fukunaga et al. (2001), four-node element
(NCP)	11	Plate/9	Not considered	NCP	11	Correia et al. (2000), 11 DOFs
(NCP)	9	Plate/9	Not considered	NCP	9	Correia et al. (2000), nine DOFs
NCP + 1	3 × NC + 3	Plate/12	Considered	NCP + 1	3 × NC + 3	Tzou and Ye (1996)
(NCP + 1)	5	Plate/4	Not considered	NCP + 1	5	Suleman and Venkaya (1995)
(1)	3	Plate/4	Not considered	1	3	Hwang and Park (1993)
2 × NCP + 1	5/3	Beam/3	Considered	2 × NCP + 1	4	Present
						Saravanos and Heyliger (1995)

Note: NCP, number of piezoelectric layers/sublayers.

The matrices and vectors in the above equation are the mechanical DOFs $q(t)$, the electrical DOFs $\phi(t)$, the mass matrix $\mathbf{M} = \int \rho \mathbf{N}^T \mathbf{N} dV$, the elastic matrix $\mathbf{K}_{qq} = \int \mathbf{B}_u^T \bar{\mathbf{C}} \mathbf{B}_u dV$, the electromechanical coupling matrix $\mathbf{K}_{q\phi} = \int \mathbf{B}_u^T \bar{\mathbf{e}} \mathbf{B}_\phi dV$, the permittivity matrix $\mathbf{K}_{\phi\phi} = \int \mathbf{B}_\phi^T \bar{\boldsymbol{\chi}} \mathbf{B}_\phi dV$, the mechanical load vector $\mathbf{F}_q = \int_V \mathbf{N}^T \mathbf{f} dV + \int \mathbf{N}^T \mathbf{F} dS + \mathbf{N}^T \mathbf{f}_c$, and the applied charge vector $\mathbf{F}_\phi = \int_S \mathbf{N}_\phi^T Q dS$.

RESULTS AND DISCUSSION

In this section, a four-layered substrate composite beam with piezoelectric bonded to its top face [pz/0°/90°/90°/0°], a three-layered cantilever beam made up of piezoelectric and non-piezoelectric materials, and a polyvinyl difluoride (PVDF) bimorph beam are analyzed using the present element. In order to evaluate this FE, the obtained results are compared with available experimental and numerical ones. Note that the polarization of the piezoelectric materials is aligned with the transverse direction of each piezoelectric layer unless stated otherwise.

For further comparison, Table 1 gives the main features of the FE formulations given in the following numerical examples: the type of FE, the number of nodes, the number of mechanical and electrical DOFs per node or element, the number of generalized unknowns, and the interlaminar continuity of the transverse shear stress are precised.

Four-Layered Substrate Composite Beam with Piezoelectric Bonded to its Top Face

In this section, a simply supported piezoelectric-laminated beam with length-to-thickness ratio $S(L/h) = 4$

(thick beam), $S = 10$ (moderately thick beam), and $S = 100$ (thin beam) is considered. This beam has the lamination scheme [pz/0°/90°/90°/0°], where pz indicates the piezoelectric layer. The substrate of the beam is made up of graphite–epoxy with the following properties:

$$(E_L, E_T, G_{LT}, G_{TT}) = (181, 10.3, 7.17, 2.87) \text{ GPa},$$

$$(\nu_{LT}, \nu_{TT}) = (0.28, 0.33)$$

L and T denote parallel and transverse directions to the fibers, respectively. The piezoelectric layer is made up of PZT-5A with the following properties:

$$(E_{11}, E_{22}, E_{33}, G_{12}, G_{23}, G_{31}) =$$

$$(61.0, 61.0, 53.2, 22.6, 21.1, 21.1) \text{ GPa},$$

$$(\nu_{12}, \nu_{13}, \nu_{23}) = (0.35, 0.38, 0.38)$$

$$(d_{31}, d_{32}, d_{33}, d_{15}, d_{24}) =$$

$$(-171, -171, 374, 584, 584) \times 10^{-12} \text{ m/V},$$

$$(\chi_{11}, \chi_{22}, \chi_{33}) = (1.53, 1.53, 1.50) \times 10^{-8} \text{ F/m}$$

The ratio of the piezoelectric layer thickness to the laminate thickness h is assumed to be 0.1. All layers of the substrate are assumed to have equal thickness. The accuracy of the proposed element is assessed by comparing the obtained result with an exact piezoelectric solution. The 3D exact solution and the aforementioned properties for graphite–epoxy and PZT-5A are issued from Kapuria (2001). In the following sensor/actuator model, all results are normalized as follows:

$$(\bar{u}_1, \bar{u}_3) = 100(u_1, u_3/S) Y_T / h S^3 p_0,$$

$$(\bar{\sigma}_{11}, \bar{\tau}_{13}) = (\sigma_{11}/S, \tau_{13}) / S p_0, \quad \bar{\phi} = 10^4 \phi Y_T d_T / h S^2 p_0$$

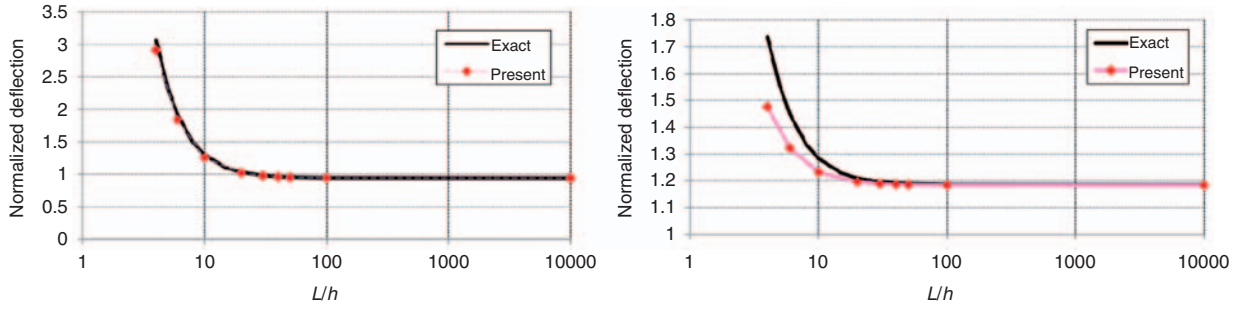


Figure 4. Distribution of the non-dimensional maximum displacement $\bar{u}_3(0.5L, 0)$ with respect to aspect ratio L/h – four-layered substrate composite [pz/0°/90°/90°/0°] left (sensory beam) – right (actuated beam).

$$(\bar{u}_1, \bar{u}_3) = 10(u_1, u_3/S)Sd_T\phi_0,$$

$$(\bar{\sigma}_{11}, \bar{\tau}_{13}) = (\sigma_{11}/10, S\tau_{13})h/Y_Td_T\phi_0$$

where $d_T = 374 \times 10^{-12} \text{ CN}^{-1}$ and $Y_T = E_T$.

Before proceeding to the detailed analysis, numerical computations are carried out for the influence of the aspect ratio (shear locking). The normalized displacement obtained at the middle of the beam is shown in Figure 4 along the exact solution for the sensor and actuator cases (see ‘Sensor model’ and ‘Actuator model’ sections for more details about the configuration). The results are in good agreement. It can be concluded that the present element is free from shear locking phenomenon.

SENSOR MODEL

A sinusoidal pressure $p(x_1) = p_0 \sin(\pi x_1/L)$ is applied on the top surface of the simply supported beam. The beam is divided into 24 elements of equal lengths. The normalized numerical results for deflection, in-plane displacement, shear stress, in-plane stress, and the induced potential at the sensory layer are given in Table 2 for three values of length-to-thickness ratio $S = 4, S = 10,$ and $S = 100$. The variation of the normalized in-plane displacement, shear stress, and in-plane stress through the thickness ($S = 4$ and $S = 10$) are shown in Figures 5 and 6. The distribution of the normalized induced potential across the sensory layer is also shown in Figure 7. It must be noted that the transverse shear stress is obtained by integrating the stress equilibrium equation through the thickness of the laminates (i.e., $\tau_{13}(z) = -\int_{-h/2}^z \sigma_{11,1} dz$) at the post-processing level.

For deflection, the present model gives results with an error rate of less than 4.3%, whatever the length-to-thickness ratio. The model predicts the in-plane displacement and in-plane stress of thin to moderately thick laminated beams with an error of less than 3.4%. The shear stress distribution obtained from the present model is in excellent agreement with the exact solution for both thin and thick laminated beams (with a maximum error rate of 2.5%). The present coupled model

Table 2. Results for the sensory beam under the pressure load.

	Sensory beam [pz/0°/90°/90°/0°]		
	Present/exact	Exact	S
$\bar{u}_3(0.5L, 0)$	0.95	-3.0636	4
	0.97	-1.2971	10
	0.99	-0.9444	100
$\bar{u}_1(0, 0.5h)$	0.86	2.4785	4
	0.96	1.6797	10
	0.99	1.5218	100
$\bar{\sigma}_{11}(0.5L, 0.5h)$	0.85	-0.5140	4
	0.96	-0.3409	10
	1.00	-0.3068	100
$\bar{\sigma}_{11}(0.5L, 0.4^-h)$	0.85	-0.8478	4
	0.96	-0.7065	10
	1.00	-0.6764	100
$\bar{\tau}_{13}(0, 0)$	1.02	-0.4063	4
	1.00	-0.4343	10
	0.99	-0.4402	100
$\bar{\phi}(0.5L, 0.5h)$	1.24	7.896	4
	1.03	7.920	10
	1.00	7.884	100

has also the capability to predict induced sensory potential with very good accuracy for thin to moderately thick laminated beams. The error rate in the predicted sensory potential is only 3.7% for moderately thick beams. The error rate approaches zero for thin beams. These results show that the prediction of the sensory behavior of thick and thin laminated beams is accurate.

ACTUATOR MODEL

An actuating potential $\phi(x_1) = \phi_0 \sin(\pi x_1/L)$ is applied at the top surface of the simply supported beam. The layered substrate composite beam and its piezoelectric layer are discretized into 24 elements of equal lengths and the thickness is divided into five numerical layers. The normalized numerical results for deflection, in-plane displacement, shear stress, and in-plane stress are compared in Table 3 for length-to-thickness ratio $S = 4, S = 10,$ and $S = 100$. The variation of

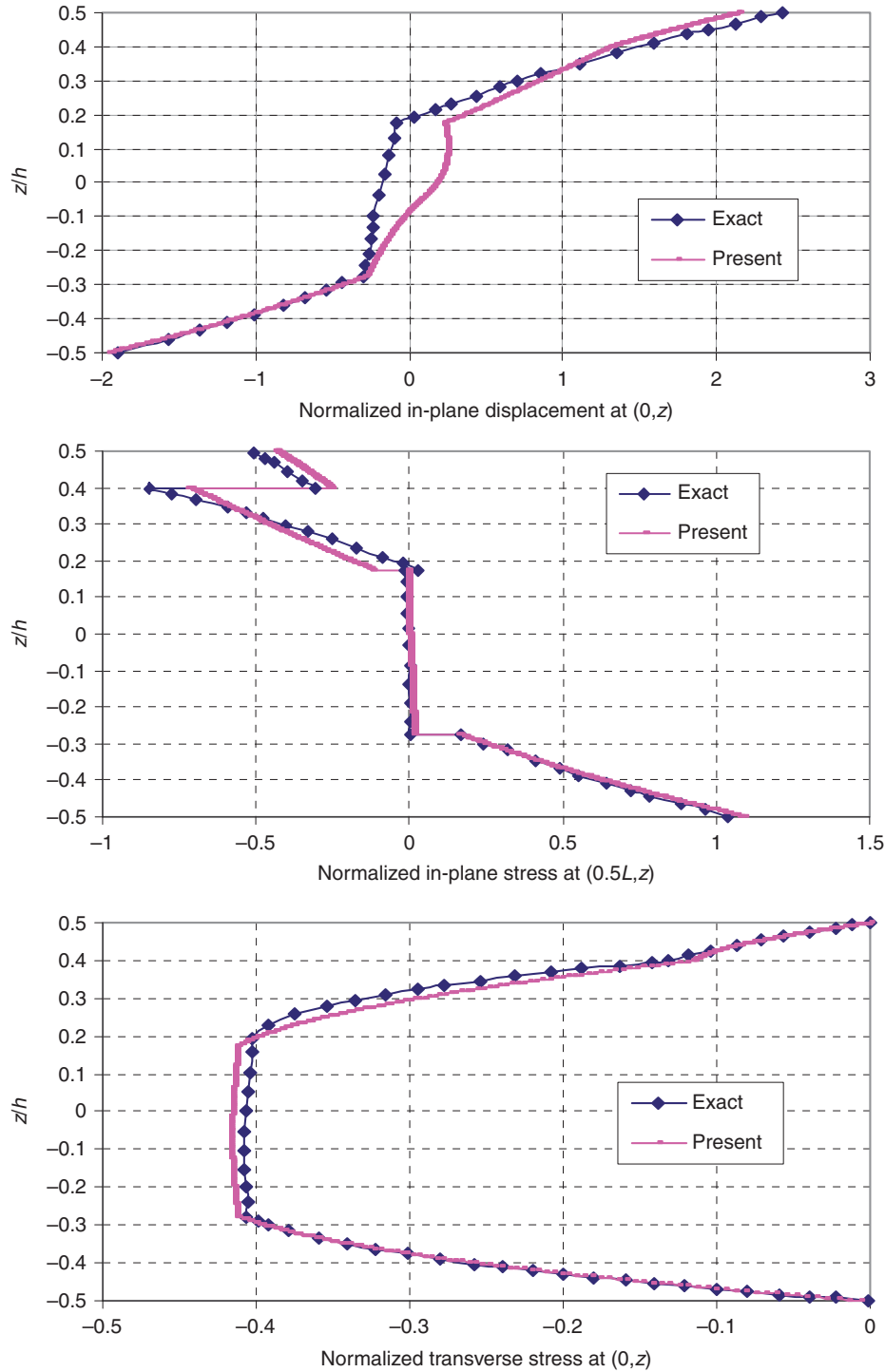


Figure 5. Distribution of \bar{u}_1 , $\bar{\sigma}_{11}$, and $\bar{\tau}_{13}$ along the thickness ($S=4$) – four-layered substrate composite $[pz/0^\circ/90^\circ/90^\circ/0^\circ]$.

the normalized in-plane displacement, shear stress, and in-plane stress through the thickness ($S=4$) are shown in Figure 8.

The model predicts the in-plane displacement, deflection, and in-plane stress of thin to moderately thick laminated beams with an error rate of less than 5%. Similar to the sensor model, the shear stress distribution

deduced from the equilibrium equation using the present model is in excellent agreement with the exact solution, even for the very thick beam, $S=4$ (the maximum error rate is 3.3%). These results demonstrate that the present model allows to predict the actuator behavior of thick and thin laminated beams accurately.

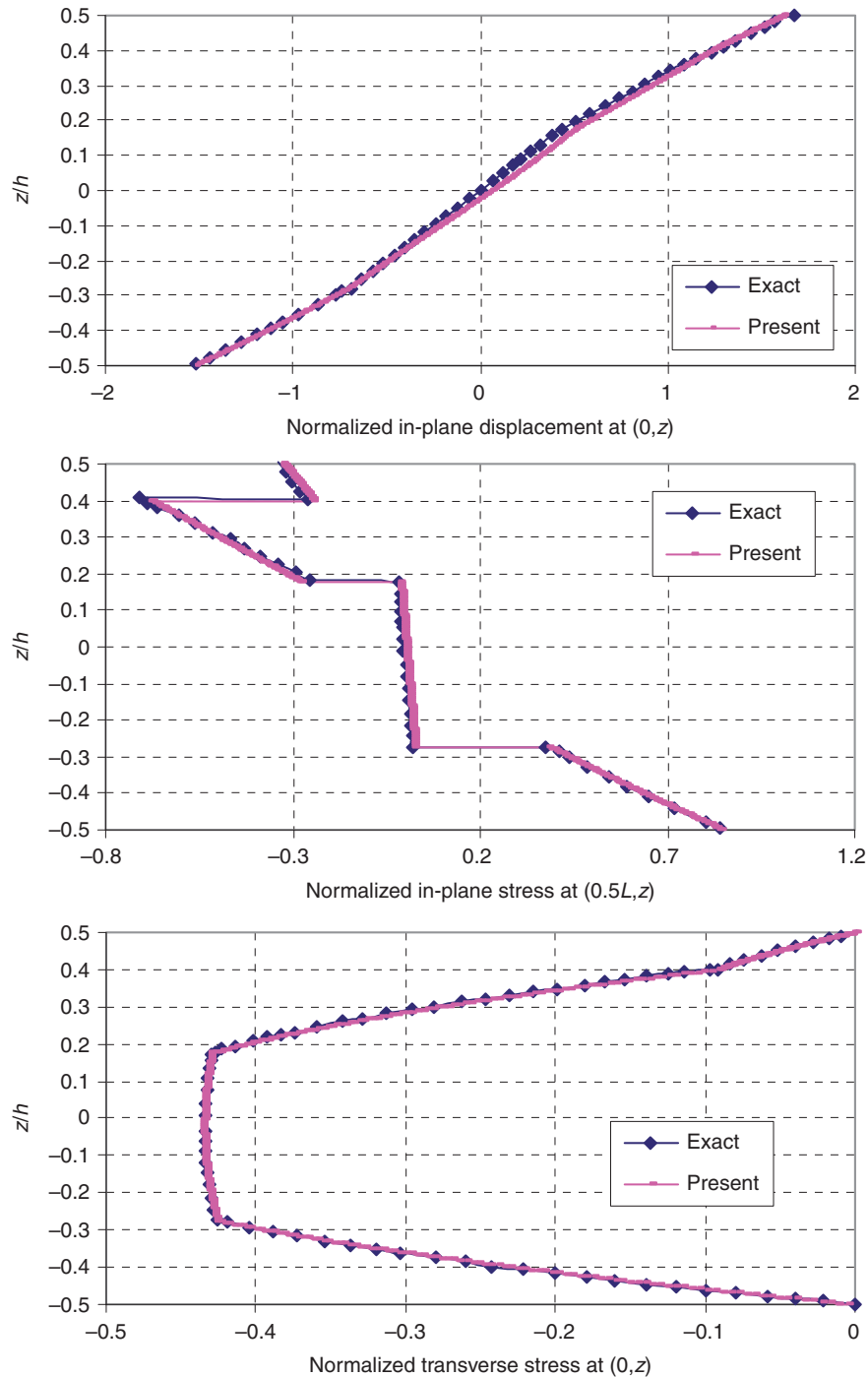


Figure 6. Distribution of \bar{u}_1 , $\bar{\sigma}_{11}$, and $\bar{\tau}_{13}$ along the thickness ($S = 10$) – four-layered substrate composite $[pz/0^\circ/90^\circ/90^\circ/0^\circ]$.

Three-Layered Cantilever Beam Made Up of Piezoelectric and Non-Piezoelectric Materials

A three-layered cantilever structure constituted by a substrate (bottom layer), adhesive (middle layer) and piezoelectric material (top layer) is considered. The substrate is made of isotropic aluminum or Gr/epoxy composite $[0^\circ]$ T300/934. The material properties and the relevant data are given in Table 4. This beam has been

studied by Saravanos and Heyliger (1995), and Chee et al. (1999). Saravanos and Heyliger applied the LW theory for all the mechanical and electrical variables. Their FE model is divided into 16/5/8 layers for the substrate/adhesive/piezoelectric materials, respectively. In the mixed model of Chee et al. (1999), the Higher Order Displacement Theory (HODT) is used for the mechanical part. As far as the electric part is concerned, the LW approach allows them to divide the thickness

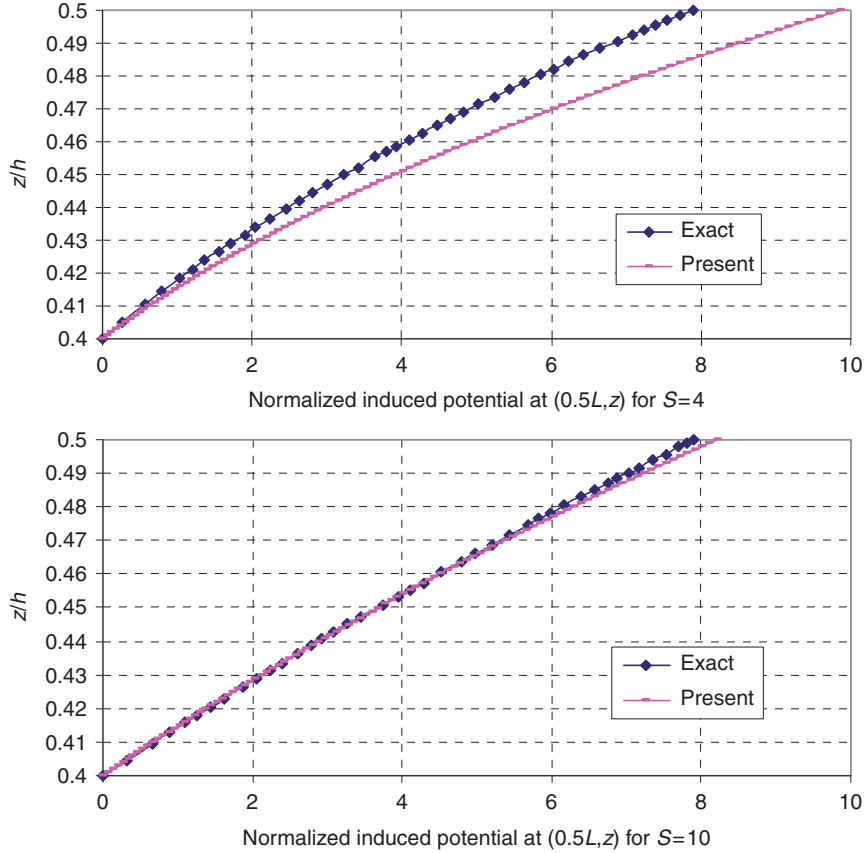


Figure 7. Distribution of the normalized sensory potential ($\bar{\phi}$) along the sensor layer – four-layered substrate composite $[pz/0^\circ/90^\circ/90^\circ/0^\circ]$.

layers into 1/1/2. The variation of the electric potential is considered as linear through each layer or sublayer. The comparison of the computational cost is given in Table 5.

THREE-LAYERED ACTIVE CANTILEVER

In order to verify the actuation capability of the presented model, a 12.5-kV current is applied across the thickness of the piezoelectric layer, which causes the beam to bend. This structure is divided into five beam elements of equal lengths, as shown in Figure 9. The piezoelectric material, the substrate, and the adhesive are modeled as one layer each. The numerical results for the present method are compared with results available from the literature in Figure 10. We can see that the present model, not only satisfies continuity condition of interlaminar displacement and transverse shear stress, but also has a high correlation with the mixed model of Chee et al. (1999).

THREE-LAYERED SENSOR CANTILEVER

In order to verify the sensory capability of our element, a load of 1000 N upward is applied to the tip of the cantilever beam. The charges generated on the piezoelectric layer cause a potential difference across the thickness which is the outcome of the electromechanical coupling

Table 3. Results for the actuated beam under sinusoidal electric potential.

	Actuated beam $[pz/0^\circ/90^\circ/90^\circ/0^\circ]$		
	Exact	Present/exact	S
$\tilde{u}_3(0.5L, 0)$	0.85	1.7370	4
	0.96	1.2837	10
	0.99	1.1866	100
$\tilde{u}_1(0, 0.5h)$	0.81	-3.638	4
	0.96	-3.017	10
	0.99	-2.890	100
$\tilde{\sigma}_{11}(0.5L, 0.5h)$	0.93	-2.032	4
	0.95	-2.144	10
	0.99	-2.167	100
$\tilde{\sigma}_{11}(0.5L, 0.4-h)$	0.84	1.617	4
	0.96	1.429	10
	0.99	1.389	100
$\tilde{\tau}_{13}(0, 0.4h)$	1.03	-6.583	4
	0.99	-6.868	10
	0.99	-6.927	100

of piezoelectric materials. Figure 11 shows the mid-plane deflections along the beam. The total voltage across the thickness of the piezoelectric is plotted in Figure 12. As shown in Figures 11 and 12, the deflection and voltage

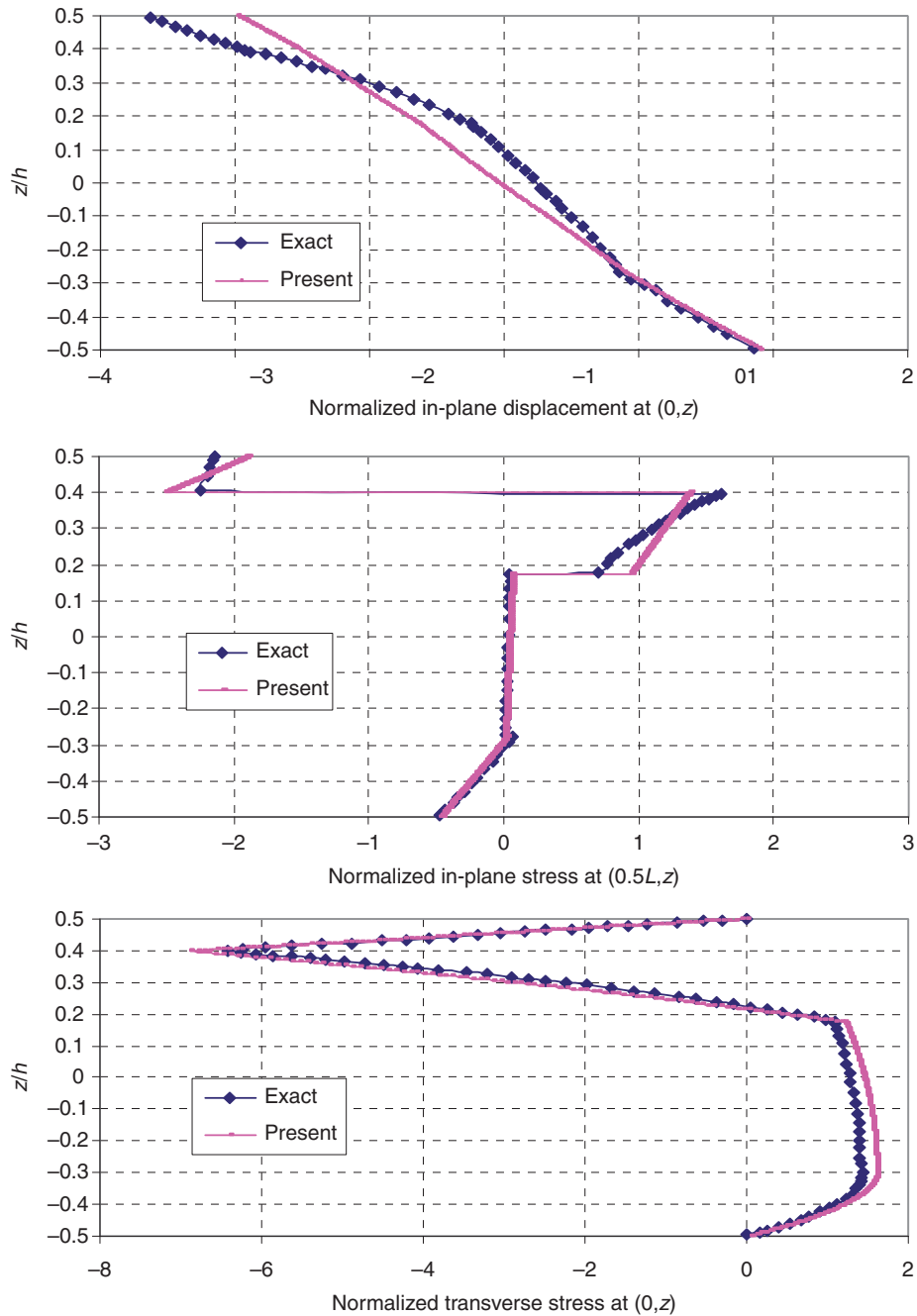


Figure 8. Distribution of \bar{u}_1 , $\bar{\sigma}_{11}$, and $\bar{\tau}_{13}$ along the thickness ($S=4$) – four-layered substrate composite $[pz/0^\circ/90^\circ/90^\circ/0^\circ]$.

distribution along the beam predicted by the present formulation have a good correlation with previous results.

PVDF Bimorph Beam

Another case study is a cantilever piezoelectric bimorph beam with two PVDF layers bonded together and polarized in opposite directions. This particular example has been analyzed among others by the following researchers: Chee et al. (1999), Hwang and Park (1993), Tzou and Ye

(1996), Tzou and Tseng (1990), Suleman and Venkayya (1995), Correia et al. (2000), and Fukunaga et al. (2001). The geometry of the bimorph beam is shown in Figure 13. The mechanical and piezoelectric properties of the PVDF are taken as: $E_{11} = E_{22} = E_{33} = 2$ GPa, $G_{12} = G_{13} = G_{23} = 1$ GPa, $\nu_{12} = \nu_{23} = \nu_{13} = 0.29$, $e_{31} = e_{32} = 0.0460$ C/m², and $\chi_{11} = \chi_{33} = 0.1062 \times 10^{-9}$ F/m. The e_{33} coefficient in all models is assumed to be zero. To assess the computational cost, a comparison of these models is given in Table 6.

Table 4. Properties for three-layered cantilever.

		PZT-4	Adhesive	T300/934	Aluminum
E_{11}	Pa	8.1300×10^{10}	6.9000×10^9	1.3238×10^{11}	6.8900×10^{10}
E_{33}	Pa	6.4500×10^{10}	6.9000×10^9	1.0760×10^{10}	6.8900×10^{10}
ν_{13}	—	0.43	0.4	0.24	0.25
G_{13}	Pa	2.5600×10^{10}	2.4600×10^9	5.6500×10^{10}	2.7600×10^{10}
D_{31}	mV ⁻¹	-1.22×10^{-10}	—	—	—
χ_{11}	FV ⁻¹	1.305965×10^{-8}	—	3.0989×10^{-11}	—
χ_{33}	FV ⁻¹	1.15102×10^{-8}	—	2.6562×10^{-11}	—
L	m	0.1524	0.1524	0.1524	0.1524
h	m	0.001524	0.000254	0.01524	0.01524
b	m	0.0254	0.0254	0.0254	0.0254

Source: Chee et al. (1999).

Table 5. Comparison of computational cost of different models for three-layered cantilever beam.

Number of DOFs					
Total	Electrical	Mechanical	Number of nodes	Number of elements	Models
1734	234	1500	26	25	Saravanos and Heyliger (1995)
38	18	20	6	5	Chee et al. (1999)
58	18	40	11	5	Present

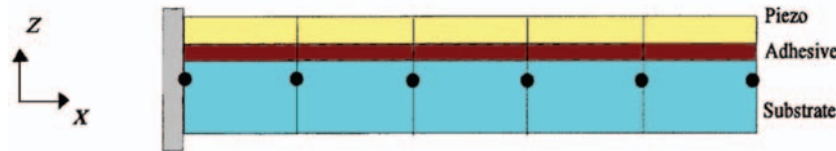


Figure 9. Three-layered actuator/sensor cantilever beam.

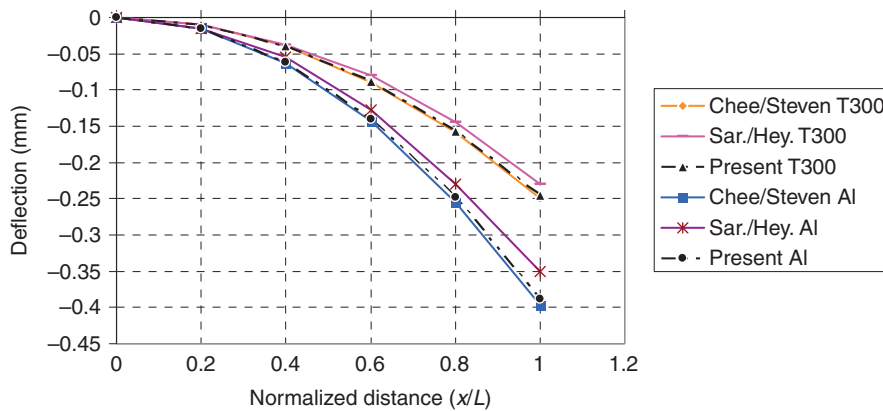


Figure 10. Deflection by piezoelectric actuation along the normalized length of the cantilever beam – actuator configuration.

ACTUATOR MODEL

In order to compare the results obtained from the present model with alternative results, the mesh is composed of five elements of same lengths. The mid-plane deflection along the beam, produced by exerting an electric potential of 1 V into the piezoelectric layers is given in Table 7. Results are also given in this table using: the results from the reduced higher order plate theory *via*

penalty functions (Fukunaga et al., 2001), the mixed FE model (Chee et al., 1999) using the Hermitian beam elements with electric potential incorporated *via* the LW formulation, the two nine-node plate elements (Correia et al., 2000) using a higher order theory (with 11 and 9 DOFs at each node, respectively), and the shell and plate elements based on FSDT (Suleman and Venkayya, 1995; Tzou and Ye, 1996). This table shows that the present

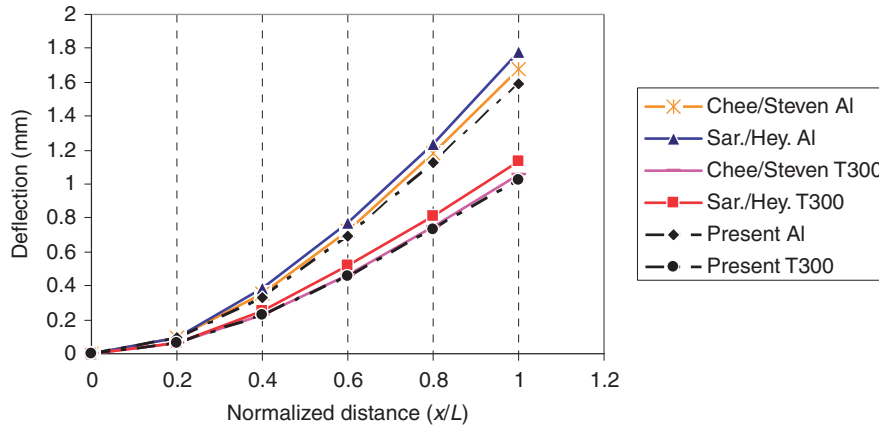


Figure 11. Deflection along the cantilever beam (load of 1000 N upward) – sensor configuration.

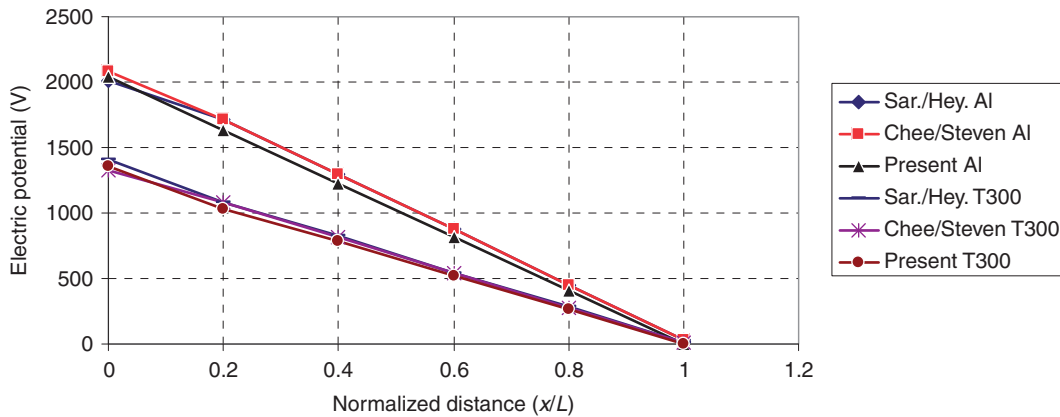


Figure 12. Voltage difference across the piezoelectric material as a function of normalized length of the cantilever beam – sensor configuration.

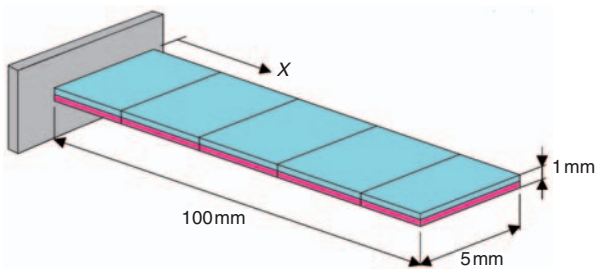


Figure 13. Cantilever piezoelectric bimorph beam.

results are in very good agreement with previous researchers' results.

SENSOR MODEL

In this section, the sensory capability is investigated. A mechanical force is applied at the free tip of the beam inducing a tip displacement equal to 10 mm. The variation of the total voltage across the thickness of the beam is plotted in Figure 14. The results are compared with the ones obtained from Chee et al. (1999), Hwang and

Park (1993), and Tzou and Tseng (1990). In the model of Hwang and Park, the sensor voltages have been measured using 5 (or 10) pieces of separate electrodes, leading to a constant voltage along each electrode and a step voltage distribution, as shown in Figure 14. However, it is possible to locate point electrodes at interested positions. Tzou and Tseng (1990) and Chee et al. (1999) measured sensor voltages distribution along the PVDF beam using these point electrodes. In the present model as well, these point electrodes has been made use. Figure 14 shows a good correlation between the results of the present model and the results of the aforementioned researchers.

CONCLUSIONS

A three-nodded beam element has been extended to the analysis of layered piezoelectric composite beams. A refined sinus model is utilized for components of the mechanical media. All displacement and stress continuities are ensured at layer interfaces as well as the free boundary conditions at the top and bottom of the beam.

Table 6. Comparison of computational cost of different models for PVDF bimorph beam.

Number of DOFs					
Total	Electrical	Mechanical	Number of nodes	Number of elements	Models
160	10	150	33	5	Fukunaga et al. (2001), nine-node element
80	10	70	12	5	Fukunaga et al. (2001), four-node element
114	24	90	36	10	Tzou and Tseng (1990)
340	10	330	33	5	Correia et al. (2000), 11 DOFs
280	10	270	33	5	Correia et al. (2000), 9 DOFs
336	66	270	33	10	Tzou and Ye (1996)
70	10	60	12	5	Suleman and Venkaya (1995)
70	10	60	22	10	Hwang and Park (1993)
38	18	20	6	5	Chee et al. (1999)
76	36	40	11	5	Present

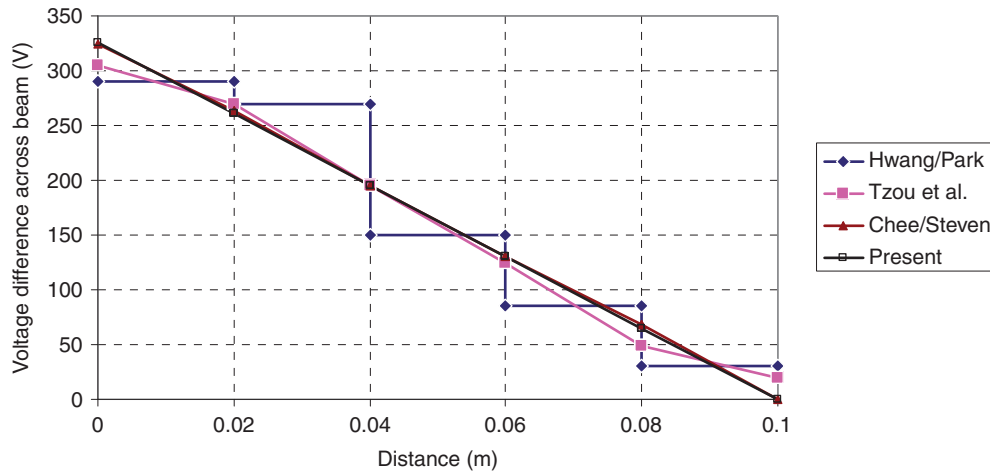


Figure 14. Voltage difference across the thickness of PVDF at various points along the length of the beam – PVDF bimorph beam – sensor configuration.

Table 7. Comparison of deflections induced by actuators – PVDF bimorph beam.

Deflections (10^{-7} m)					
100	80	60	40	20	Location x (mm)
3.45	2.208	1.242	0.552	0.138	Present
3.45	2.208	1.242	0.552	0.138	Mixed model (Chee et al., 1999)
3.45	2.21	1.24	0.553	0.139	Plate FE (nine-node element) (Fukunaga et al., 2001)
3.45	2.21	1.24	0.553	0.139	Plate FE (four-node element) (Fukunaga et al., 2001)
3.45	2.21	1.24	0.552	0.138	Theory (Tzou and Tseng, 1990)
3.45	2.21	1.24	0.552	0.138	Plate FE (11 DOFs) (Correia et al., 2000)
3.45	2.21	1.24	0.552	0.138	Plate FE (nine DOFs) (Correia et al., 2000)
3.30	2.11	1.19	0.528	0.132	Shell FE (FDST) (Tzou and Ye, 1996)
3.45	2.21	1.24	0.55	0.14	Plate FE (FDST) (Suleman and Venkaya, 1995)
3.16	2.02	1.14	0.51	0.13	Analytical (Correia et al., 2000)
3.15	–	–	–	–	Experimental (Tzou and Tseng, 1990)

This conforming FE does not need shear correction factor, and the number of its mechanical unknowns is independent of the number of layers. Concerning the electrical part, a high-order approximation for the electrical potential ensures the boundary condition for the applied voltage.

In order to evaluate sensor and actuator capabilities of this element, a four-layered substrate composite beam with piezoelectric bonded to its top face, a three-layered cantilever beam equipped with piezoelectric and non-piezoelectric materials, and a PVDF bimorph beam have been considered. The numerical results obtained from this formulation have been compared with results available in the open literature. Good correlation has been found. The present FE is very useful in modeling thin and thick piezoelectric composite beams under mechanical and electrical loads.

This element seems to be a good compromise between the computational cost and the accuracy of results for a wide field of applications.

REFERENCES

- Allik, H. and Hughes, T.J.R. 1970. "Finite Element Method for Piezoelectric Vibration," *International Journal for Numerical Methods in Engineering*, 2:151–157.
- Ambartsumyan, S.A. 1969. *Theory of Anisotropic Plates*, Technomic, Stamford, CT (Translated from Russian by T. Cheron).
- Benjeddou, A. 2000. "Advances in Piezoelectric Finite Element Modeling of Adaptive Structural Elements: A Survey," *Computers and Structures*, 76:347–363.
- Carrera, E. 2003. "Historical Review of Zig-Zag Theories for Multilayered Plates and Shells," *Applied Mechanics Review*, 56:287–308.
- Carrera, E. and Boscolo, M. 2007. "Classical and Mixed Elements for Piezoelectric Plates," *International Journal for Numerical Methods in Engineering*, 70:1135–1181.
- Carrera, E. and Brischetto, S. 2007. "Reissner Mixed Theorem Applied to Static Analysis of Piezoelectric Shells," *Journal of Intelligent Material Systems and Structures*, 18:1083–1181.
- Carrera, E. and Nali, P. 2009. "Mixed Piezoelectric Plate Elements with Direct Evaluation of Transverse Electric Displacement," *International Journal for Numerical Methods in Engineering*, 80:403–424.
- Chee, C.Y.K., Tong, L. and Steven, P.G. 1999. "A Mixed Model for Composite Beams With Piezoelectric Actuators and Sensors," *Smart Materials and Structures*, 8:417–432.
- Chopra, I. 2002. "Review of State of Art of Smart Structures and Integrated Systems," *AIAA Journal*, 40(11):2145–2187.
- Correia, F.V.M., Gomes, M.A.A., Suleman, A., Mota Soares, C.M. and Mota Soares, C.A. 2000. "Modeling and Design of Adaptive Composite Structures," *Computer Methods in Applied Mechanics and Engineering*, 185:325–346.
- Crawley, E.F. and de Luis, J. 1987. "Use of Piezoelectric Actuators as Element of Intelligent Structures," *AIAA Journal*, 25:1373–1385.
- D'Ottavio, M. and Kröplin, B. 2006. "An Extension of Reissner Mixed Variational Theorem to Piezoelectric Laminates," *Mechanics of Advanced Materials and Structures*, 13:139–150.
- Dau, F., Polit, O. and Touratier, M. 2004. "An Efficient C^1 Finite Element with Continuity Requirements for Multilayered/Sandwich Shell Structures," *Computers and Structures*, 82:1889–1899.
- Fernandes, A. and Pouget, J. 2003. "Analytical and Numerical Approaches to Piezoelectric Bimorph," *International Journal of Solids and Structures*, 40:4331–4352.
- Fukunaga, H., Hu, N. and Ren, G.X. 2001. "Finite Element Modeling of Adaptive Composite Structures Using a Reduced Higher-Order Plate Theory Via Penalty Functions," *International Journal of Solids and Structures*, 38:8735–8752.
- Garcia Lage, R., Mota Soares, C.M., Mota Soares, C.A. and Reddy, J.N. 2004a. "Analysis of Adaptive Plate Structures by Mixed Layerwise Finite Elements," *Composite Structures*, 66:269–276.
- Garcia Lage, R., Mota Soares, C.M., Mota Soares, C.A. and Reddy, J.N. 2004b. "Modeling of Piezolaminated Plates Using Layerwise Mixed Finite Element Models," *Computers and Structures*, 82:1849–1863.
- Gaudenzi, P. 2009. *Smart Structures: Physical Behaviour, Mathematical Modeling and Applications*, John Wiley & Sons, Chichester.
- Heyliger, P.R. and Saravanos, D.A. 1994. "Coupled Discrete-Layer Finite Elements for Laminated Piezoelectric Plates," *Communications in Numerical Methods in Engineering*, 10:971–981.
- Hwang, W.S. and Park, H.C. 1993. "Finite Element Modeling of Piezoelectric Sensors and Actuators," *AIAA Journal*, 31:930–937.
- Jiang, J.P. and Li, D.X. 2007. "A New Finite Element Model for Piezothermoelastic Composite Beam," *Journal of Sound and Vibration*, 306:849–864.
- Kapurja, S. 2001. "An Efficient Coupled Theory for Multilayered Beams with Embedded Piezoelectric Sensory and Active Layers," *International Journal of Solids and Structures*, 38:9179–9199.
- Kapurja, S. 2004. "Higher Order Zig-Zag Theory for Fully Coupled Thermo-Electric-Mechanical Smart Composite Plates," *International Journal of Solids and Structures*, 41:1331–1356.
- Kapurja, S. and Alam, N. 2006. "Efficient Layerwise Finite Element Model for Dynamic Analysis of Laminated Piezoelectric Beams," *Computer Methods in Applied Mechanics and Engineering*, 195:2742–2760.
- Kusculuoglu, Z.K., Fallahi, B. and Royston, T.Y. 2004. "Finite Element Model of a Beam With a Piezoelectric Patch Actuator," *Journal of Sound and Vibration*, 276:27–44.
- Li, X. and Liu, D. 1997. "Generalized Laminated Theories Based on Double Superposition Hypothesis," *International Journal for Numerical Methods in Engineering*, 40:1197–1212.
- Mitchell, J.A. and Reddy, J.N. 1995. "A Refined Plate Theory for Composite Laminates with Piezoelectric Laminate," *International Journal of Solids and Structures*, 32:2345–2367.
- Oh, J. and Cho, M. 2004. "A Finite Element Based on Cubic Zig-Zag Plate Theory for the Prediction of Thermo-Electric-Mechanical Behaviors," *International Journal of Solids and Structures*, 41:1357–1375.
- Ossadzow-David, C. and Touratier, M. 2004. "A Multilayered Piezoelectric Shell Theory," *Composites Science and Technology*, 64:2121–2137.
- Plagianakos, T.S. and Saravanos, D.A. 2005. "Coupled High-Order Shear Layerwise Analysis of Adaptive Sandwich Piezoelectric Composite Beams," *AIAA Journal*, 43:885–894.
- Polit, O. and Bruant, I. 2006. "Electric Potential Approximations for an Eight Node Plate Finite Element," *Computers and Structures*, 84:1480–1493.
- Polit, O. and Touratier, M. 2000. "High-Order Triangular Sandwich Plate Finite Element for Linear and Non-linear Analyses," *Computer Methods in Applied Mechanics and Engineering*, 185:305–324.
- Polit, O., Touratier, M. and Lory, P. 1994. "A New Eight-Node Quadrilateral Shear Bending Plate Finite Element," *International Journal for Numerical Methods in Engineering*, 37:387–411.

- Reddy, J.N. 1993. "An Evaluation of Equivalent-Single-Layer and Layerwise Theories of Composite Laminates," *Composite Structures*, 25:21–35.
- Robaldo, A., Carrera, E. and Benjeddou, A. 2006. "A Unified Formulation for Finite Element Analysis of Piezoelectric Adaptive Plates," *Computers and Structures*, 84:1494–1505.
- Saravanos, D.A. and Heyliger, P.R. 1995. "Coupled Layer-Wise Analysis of Composite Beams with Embedded Piezoelectric Sensors and Actuators," *Journal of Intelligent Material Systems and Structures*, 6:350–363.
- Saravanos, D.A. and Heyliger, P.R. 1999. "Mechanics and Computational Models for Laminated Piezoelectric Beams, Plates, and Shells," *Applied Mechanics Review*, 52:305–319.
- Saravanos, D.A., Heyliger, P.R. and Hopkins, D.A. 1997. "Layer-Wise Mechanics and Finite Element Model for the Dynamic Analysis of Piezoelectric Composite Plates," *International Journal of Solids and Structures*, 34:359–378.
- Semedo Garcao, J.E., Mota Soares, C.M., Mota Soares, C.A. and Reddy, J.N. 2004. "Analysis of Laminated Adaptive Plate Structures Using Layer-Wise Finite Element Models," *Computers and Structures*, 82:1939–1959.
- Sheikh, A.H., Topdar, P. and Halder, S. 2001. "An Appropriate FE Model for Through Thickness Variation of Displacement and Potential in Thin/Moderately Thick Smart Laminates," *Composite Structures*, 51:401–409.
- Shu, X. 2005. "Free-Vibration of Laminated Piezoelectric Composite Plates Based on an Accurate Theory," *Composite Structures*, 67:375–382.
- Suleman, A. and Venkayya, V.B. 1995. "A Simple Finite Element Formulation for a Laminated Composite Plate with Piezoelectric Layers," *Journal of Intelligent Material Systems and Structures*, 6:776–782.
- Sung, C.K., Chen, T.F. and Chen, S.G. 1996. "Piezoelectric Modal Sensor/Actuator Design for Monitoring/Generating Flexural and Torsional Vibrations of Cylindrical Shells," *Journal of Sound and Vibration*, 118:48–55.
- Thornburgh, R.P. and Chattopadhyay, A. 2002. "Simultaneous Modeling of Mechanical and Electrical Response of Smart Composite Structures," *AIAA Journal*, 40:1603–1610.
- Touratier, M. 1991. "An Efficient Standard Plate Theory," *International Journal of Engineering Science*, 29:901–916.
- Tzou, H.S. and Gadre, M. 1989. "Theoretical Analysis of a Multi-Layered Thin Shell Coupled with Piezoelectric Shell Actuators for Distributed Vibration Controls," *Journal of Sound and Vibration*, 132:433–450.
- Tzou, H.S. and Tseng, C.I. 1990. "Distributed Piezoelectric Sensor/Actuator Design for Dynamic Measurement/Control of Distributed Parameter Systems: A Piezoelectric Finite Element Approach," *Journal of Sound and Vibration*, 138:17–34.
- Tzou, H.S. and Ye, R. 1996. "Analysis of Piezoelectric Structures with Laminated Piezoelectric Triangle Shell Elements," *AIAA Journal*, 34:110–115.
- Vidal, P. and Polit, O. 2006. "A Thermo-Mechanical Finite Element for the Analysis of Rectangular Laminated Beams," *Finite Elements in Analysis and Design*, 42:868–883.
- Vidal, P. and Polit, O. 2008. "A Family of Sinus Finite Elements for the Analysis of Rectangular Laminated Beams," *Composite Structures*, 84:56–72.
- Vidal, P. and Polit, O. 2009. "A Refined Sine-Based Finite Element with Transverse Normal Deformation for the Analysis of Laminated Beams Under Thermomechanical Loads," *Journal of Mechanics of Material and Structures*, 4:1127–1155.
- Wang, B.T. and Rogers, C.A. 1991. "Laminate Plate Theory for Spatially Distributed Induced Strain Actuators," *Journal of Composite Materials*, 25:433–452.
- Wang, S.Y. 2004. "A Finite Element Model for the Static and Dynamic Analysis of a Piezoelectric Bimorph," *International Journal of Solids and Structures*, 41:4075–4096.
- Xu, K.M., Noor, A.K. and Tang, Y. 1995. "Three-Dimensional Solutions for Coupled Thermo-Electro-Elastic Response of Multi-Layered Plates," *Computer Methods in Applied Mechanics and Engineering*, 126:355–371.

APPENDIX

The coefficients A_k , B_k , C_k , D_k , E_k , F_k , H_k and I_k are given below:

$$A_k = \frac{f'(z_k)(G_k - G_{k-1})}{2G_k a_k}$$

$$E_k = A_k$$

$$B_k = \frac{(-G_{k-1} a_{k-1} - 3G_k a_k)}{2G_k a_k}$$

$$F_k = \frac{(-G_{k-1} a_{k-1} - G_k a_k)}{2G_k a_k}$$

$$C_k = \frac{(-3G_{k-1} a_{k-1} - 3G_k a_k)}{2G_k a_k}$$

$$H_k = \frac{(-3G_{k-1} a_{k-1} - G_k a_k)}{2G_k a_k}$$

$$D_k = \frac{(6G_{k-1} a_{k-1} + 6G_k a_k)}{2G_k a_k}$$

$$I_k = D_k$$